Materials Today Chemistry 24 (2022) 100824

Contents lists available at ScienceDirect

Materials Today Chemistry

journal homepage: www.journals.elsevier.com/materials-today-chemistry/

Heterostructured composite of NiFe-LDH nanosheets with Ti_4O_7 for oxygen evolution reaction

K.B. Ibrahim [a], W.-N. Su [a, *], M.-C. Tsai [b], A.W. Kahsay [b], S.A. Chala [b], M.K. Birhanu [b], J.-F. Lee [c], B.J. Hwang [b, c, **]

[a] Nano-electrochemistry Laboratory, Graduate Institute of Applied Science and Technology, National Taiwan University of Science and Technology, Taipei 106, Taiwan
[b] Nano-electrochemistry Laboratory, Department of Chemical Engineering, National Taiwan University of Science and Technology, Taipei, 106, Taiwan
[c] National Synchrotron Radiation Research Center, Hsin-Chu, 300, Taiwan

ARTICLE INFO

Article history:
Received 16 October 2021
Received in revised form
14 January 2022
Accepted 29 January 2022
Available online 18 March 2022

Keywords:
Layered double hydroxides
Charge transfer effect
Structural deformation
Oxide support
Defects

ABSTRACT

Developing oxygen evolution reaction (OER) electrocatalyst based on earth-abundant materials holds great promise for ascertaining water-splitting to surmount its deprived kinetics. In this regard, NiFe-LDH (layered double hydroxide) receives considerable attention owing to their layered structure. However, they still suffer from poor electronic conductivity and structural stability. We combined NiFe-LDH nanosheets with Magnéli phase Ti_4O_7 into a heterostructured composite. A series of analyses reveal that decorating Ti_4O_7 facilitates charge transfer to enhance the conductivity of NiFe-LDH-Ti_4O_7. During electrochemical measurement, Ni^{2+} is transformed to metastable Ni^{3+} (Ni (OH)→ NiOOH) before the OER onset potential. Thus, the presence of Ni^{3+} as the main active sites could improve the chemisorption of OH^- to facilitate OER. As a result, the NiFe-LDH-Ti_4O_7 catalyst delivers as low as onset potential (1.43 V). Combining the holey structure (NiFe-LDH and Ti_4O_7) and the defect engineering generated on NiFe-LDH-Ti_4O_7 as a synergistic effect improves the OER performance. The inclusion of Ti_4O_7 in the composite leads to more vacancy sites, as evidenced by the extended X-ray absorption fine structure (EXAFS) analysis. The obtained defective structure with a low coordination environment would improve the electronic conductivity and facilitate the adsorption process of H_2O onto metal cations, thereby increasing the intrinsic catalytic activity of NiOOH. The strong coupling of NiFe-LDH and Ti_4O_7 also increases the stability, and the heterostructured composite helps maintain the structural robustness of the LDH.

1. Introduction

The world has never needed energy more than it does today. The quest for abundant, convenient, and sustainable energy sources continues to be the primary concern to confront the ever-increasing standard of living [1]. The principal energy source across the globe is fossil fuels, which are rapidly depleted. In addition to the limited resources, the problem is further intensified by the growing world population and global warming due to CO_2 emissions from fossil fuel combustion [1–3]. Owing to its high energy density and non-polluting characteristics, water splitting is considered an important pathway to produce spotless energy and substantially increase the share of renewable energy sources for powering the globe [4–8]. However, the oxygen evolution reaction (OER) with sluggish kinetics has remained a grand bottleneck to realize efficient water-splitting technologies meeting the desired goals. Even the conventionally accepted benchmark catalysts such as IrO_2 and RuO_2 are not satisfactory in catalyzing OER, not to mention their scarcity and high cost [9]. OER also plays a pivotal role in achieving rechargeable metal–air batteries [5]. This necessitates the exploration of catalysts driving OER at a lower overpotential and faster kinetics. In this regard, metal oxides/double-layer hydroxides have been acknowledged for their promising performances in ORR [10], OER [11]. However, they are challenged by their intrinsically poor conductivity, impeding the electron transfer rate and thereby jeopardizing the entire catalytic activity [12].

* Corresponding author.
** Corresponding author.
E-mail addresses: wsu@mail.ntust.edu.tw (W.-N. Su), bjh@mail.ntust.edu.tw (B.J. Hwang).

https://doi.org/10.1016/j.mtchem.2022.100824
2468-5194/

Recently, layered double hydroxides are excellent alternatives in this field. Among them, Ni-based LDH materials have attracted significant interest since Considering the effective charge transport, appreciable stability, immensely exposed active surface sites, composed of materials that are found naturally on earth, and because they exhibit impressive catalytic activity [12,13]. Despite the great progress, low conductivity and self-aggregation are still the current primary issues for NiFe-LDHs, which inhibit the optimization of electrocatalytic performances.

Lately, strategies have been developed to overcome these problems, such as creating three-dimensional (3D) nanostructures, [14] or adjusting the cation valences, or stacking the structure of LDH [15]. Carbon support has important featuring like low cost, high surface area, and conductivity, making it a popular material in various electrocatalytic systems [16–19]. However, poor stability caused by carbon corrosion and the predominance of weak contacts among support and catalyst leads to the agglomeration and detachment of catalyst from support. These also lead to a consequent decrement in active surface area and loss in activity after long-term operation [20]. Researchers have designed robust non-carbon support materials, such as conductive and stable metal oxide support, to avoid the issue of carbon corrosion [21–23], to introduce a synergistic co-catalytic, and to create metal and oxygen vacancy [10,24]. Therefore, blending LDH with metal oxide enhances the stability of the material in an alkaline electrolyte, primarily when the conductive Ti_4O_7 instead of TiO_2 is employed.

With this outlook, we systematically investigated combining the NiFe-LDHs and Ti_4O_7 (NiFe-LDH-Ti_4O_7) as high-performance and stable catalysts for OER. Based on the above contemplations, it is hoped that the heterostructured composite of NiFe-LDHs on Ti_4O_7 has several additional effects. (i) Decorated Ti_4O_7 can increase the oxygen vacancies on the interface to improve OER catalytic activity. (ii) The poor electronic conductivity of LDHs can be improved via catalyst−support interactions. (iii) The electronic coupling and structural defects caused by the composite are testified by the X-ray absorption spectroscopy (XAS) technique. Furthermore, how these features are translated into actual catalytic performance is of major concern. It is envisaged that the suggested heterostructured composite offers a new strategy and understanding in developing intrinsically highly active, stable, and robust OER electrocatalysts.

2. Experimental section

2.1. Synthesis of Ti_4O_7 as catalyst support

Ti_4O_7 was synthesized by dissolving TiO_2 with ethanol and followed by (3-aminopropyl) trimethoxysilane. The pH of the solution was maintained by adding NH_3. Then, tetraethylorthosilicate was added under continuous stirring. The synthesized material was collected through centrifuged, repeatedly washed, filtered, and dried at 80 °C. Afterward, the sample was ready to reduce with pure H_2 [10]. Finally, SiO_2 was removed through etching Ti_4O_7 with HF.

2.2. Synthesis of NiFe-LDH

NiFe-LDH was prepared with a hydrothermal method at 120 °C for 12 h. Then, the resulting powder NiFe-LDH was washed and dried at 80 °C [25]. To prepare NiFe-LDH-Ti_4O_7, Ti_4O_7 was added and followed the same procedure for NiFe-LDH synthesis. The detailed procedures, characterization methods, techniques about the electrochemical measurements are summarized in the supplementary information.

2.3. Characterization

The crystal structure of the sample was studied by using an X-ray diffractometer (Bruker D2 Phaser XRD machine, equipped with a Cu-Kα irradiation photon source (λ = 1.5406 Å, Ni filter, 40 kV, and 100 mA). Morphologies and elemental analysis of the samples were examined using a field emission scanning electron microscope (FESEM, JEOL 7600 F) equipped and an energy dispersive spectroscope (EDX).

Electrochemical measurements were implemented with Ni-foam (diameter: 5 mm; 1.6 mm thickness) in a three-electrode setup. The catalyst ink for the Ni-foam test was prepared by dispersing 0.014 g of the sample into 1 ml (4:1) solution of IPA: H_2O: 5% Nafion. The ink was drop-cast onto a Ni-foam tip to attain a mass loading of 0.2 mg cm^{-2}. Ni-foam, graphite counter electrode, and Ag/AgCl (3 M KCl) reference electrode were immersed in 1 M KOH previously purged by O_2. The catalytic activity of the samples was investigated via cyclic voltammetry (CV) and linear sweep voltammetry (LSV). CV was carried out at a scan rate of 5 mV/s. The samples were cycled about 20 times until stable CV curves were obtained. LSV was performed at a scan rate of 1 mV/s to get polarization curves. Commercial carbon paper (CeTech Co. Ltd., Taiwan; 0.18 mm thick and batch number 201120) was adopted for the durability test with a fixed reaction area of 1 cm^2. The carbon was rinsed with IPA before use without any further pretreatment.

2.4. Electrochemical impedance spectroscopy

The ohmic resistance (R_Ω) (which includes resistance from components such as the electrolyte and electrode) and the charge transfer resistance (R_{ct}) of electrocatalysts were determined from electrochemical impedance spectroscopy (EIS), whose frequency ranged from 100 mHz to 100 kHz (amplitude = 10 mV). EIS was conducted using a computer-controlled potentiostat (PGSTAT302 N, Metrohm Autolab) assembled with a rotational system (Pine Research Instrumentation, Durham, NC, U.S.A.) in 1 M KOH electrolyte solution at 25 °C and ~1.45 V (vs. RHE), which is the typical potential used for assessing the electrochemical activity of the electrocatalyst for OER. The total mass loading was 1 mg/cm^2.

3. Result and discussion

3.1. Materials characterization

The LDH ink was directly cast on Ni-foam to measure electrochemical performance. Ni-foam was adopted due to its high electronic conductivity. More importantly, it could minimize the oxygen bubble and facilitate electrolyte diffusion across the active catalyst. The individual images of as-prepared NiFe-LDH and Ti_4O_7 are seen in Fig. 1a and b. The morphology of the NiFe-LDH-Ti_4O_7 composite, characterized by SEM in Fig. 1c, shows a well-aligned LDH nanosheet structure uniformly decorated by Ti_4O_7. It further confirms that the decoration of Ti_4O_7 did not change the morphology and crystal size of NiFe-LDH. EDS analysis in Fig. S2 validates Ni and Fe's existence in an atomic ratio of 3:1, showing their uniform distribution in the NiFe-LDH-Ti_4O_7 nanosheets.

The crystal structure of NiFe-LDH exhibits a series of Bragg diffraction that best fits with NiFe-LDH is assigned to JCPDF#89–7111. The XRD graph depicted in Fig. 1d confirms no impurity phases after decorating Ti4O7. It also shows that the supporting material does not diffuse into the interlayered structure of LDH meanwhile. The Raman spectra in Fig. 1e show the peaks are correlated with a representative nitrate-intercalated NiFe-LDH, such as $\nu(NO_3^-)$ at 1500 cm^{-1}. Raman peaks at 470 cm^{-1} and 565 cm^{-1} are assigned to M-O-M, M−OH, and M−O vibrations.

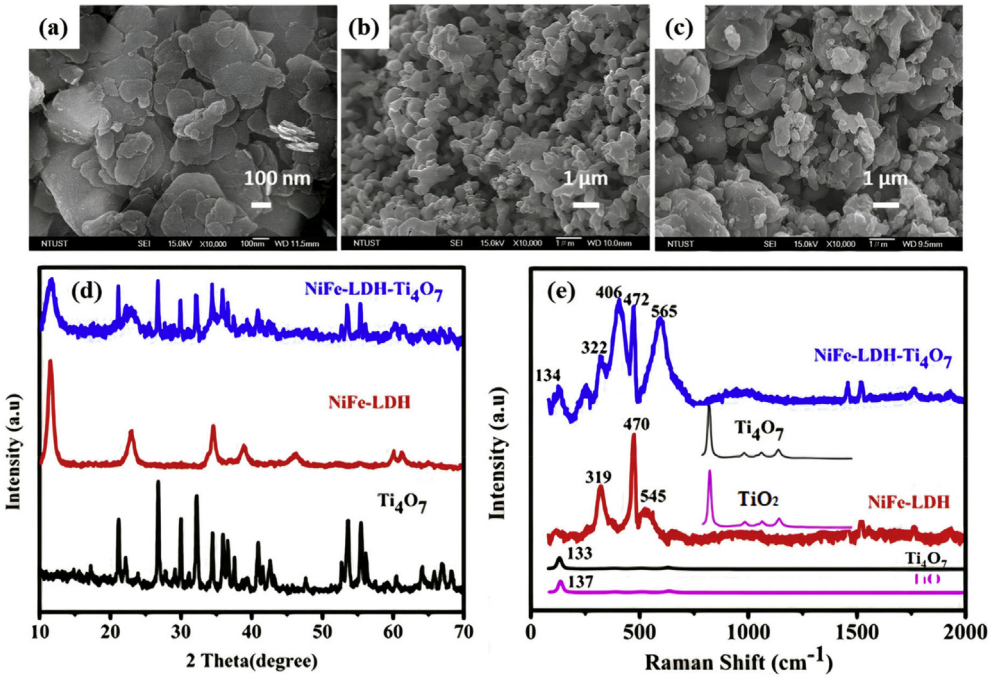

Fig. 1. SEM images for (a) NiFe-LDH (b) Ti4O7, and (c) NiFe-LDH-Ti4O7 composite; (d) XRD patterns of NiFe-LDH, Ti_4O_7, and NiFe-LDH-Ti_4O_7; (e) Raman spectra of as-prepared NiFe-LDH and Ti_4O_7 at smaller ranges.

Compared to NiFe-LDH, NiFe-LDH-Ti_4O_7 shows a visible red-shift of the band ascribed to the O−M−O and O−M bending, likely caused by crystal defects [26]. Meanwhile, the strong and weak peaks at high wavenumbers at 3580 cm^{-1} and 2950 cm^{-1} shown in Fig. S3c were attributed to the stretching mode of OH bonds in the hydroxide layer and H_2O. It further proves the intercalation of OH^- ion and water molecule, respectively. FTIR measurement was also conducted to confirm the intercalation of anions (Fig. S3d). LDH material shows a sharp peak at 1366 cm^{-1} and confirms the stretching vibration of the interlayer NO_3^- ions. The bands in the low-frequency region, approximately 700 $cm^{-1,}$ belong to M-O-M (Fe/Ni−O, and Ni/Fe−O−Fe) vibrations of the layer cations of LDH. The broad shoulder band near 3500 cm^{-1} may be ascribed to the O−H group stretching vibration from the interlayer water molecules and hydroxide layers. The vibration at 1630 cm^{-1} is attributed to the angular deformation mode of H_2O molecules. Therefore, FTIR measurement combined with Raman confirms the formation of NiFe- LDH with interlayer anions that play their parts in OER activity.

The change in electronic structure, surface chemical state, elemental information, and interaction amongNiFe-LDH-Ti_4O_7 was examined by XPS. The full wide-range spectra (Fig. S4) first confirm the co-existence of Ni, Fe, Ti, and O in the as-synthesized material in their respective binding energy. Concerning the individual spectra for Ni, Fe, and Ti, as depicted in Fig. 2, the Ni 2p spectrum shows deconvoluted into four peaks, confirming the split of 2p orbital into $2p_{1/2}$ and $2p_{3/2}$ doublets due to spin-orbit coupling. The band center of Ni 2p at 859.3 eV and 876.9 eV homologous to Ni $2p_{3/2}$ and Ni $2p_{1/2}$, respectively in Fig. 2a, imparts the presence of Ni^{2+} in NiFe-LDH. However, the Ni 2p orbital in NiFe-LDH-Ti_4O_7 shifts by 1.3 eV to higher binding energy than the Ni 2p spectrum in the NiFe-LDH, suggesting the Ni^{2+} was oxidized into Ni [3]+. Similarly, the appearance of two distinct peaks at 714.5 eV and 727.2 eV in Fig. 2b corresponds to Fe^{3+} $2p_{1/2}$ and Fe^{3+} $2p_{3/2}$, respectively. Noticeably, the BE for the peaks of Fe $2p_{3/2}$ and Fe $2p_{1/2}$ in NiFe-LDH-Ti_4O_7 shows a slightly negative shift compared to Fe 2p spectrum in NiFe-LDH. However, the BE of Ti $2p_{3/2}$ (458.4 eV) in NiFe-LDH-Ti_4O_7 shifts to a lower binding energy position compared to the Ti $2p_{3/2}$ in Ti_4O_7, as seen in Fig. 2c. This could be attributed to the presence of corundum Ti_2O_3 (Ti^{3+}) or oxygen vacancies in the composite and the electronic coupling, i.e., charge transfer, between the supporting Ti_4O_7 oxide and the NiFe-LDH. Similarly, a shoulder peak at a lower energy of 456.0 eV in NiFe-LDH-Ti_4O_7 (Fig. 2c) can be attributed to the existence of the valence state of Ti^{2+} ions. It has been suggested that electronic coupling could play an important role in OER catalysts, such as NiMn-LDH and Ag nanowires [14] and NiRu-LDH [10]. In the following, how this effect in the heterostructure composite could affect the OER activity will be discussed.

3.2. XANES and EXAFS analysis of the heterostructured composite

X-ray absorption spectroscopy was conducted at the beamline station 17C, NSRRC, Taiwan, to investigate the interaction between NiFe-LDH and Ti_4O_7, variation in oxidation state, and local symmetry of metal ions. The structural and electronic effects are gathered from EXAFS and XANES, respectively. The threshold energy position of the K-edge XANES spectra of the transition metals is sensitive to their oxidation states. At the same time, the shape of the peaks is sensitive to the local structural environment of the absorbing element. Based on this, Ni, Fe, and Ti K-edge XANES spectra are characterized by three common parts, i.e., edge jump (*1s → 3d)*, main edge (dipole transition *1s → 4p)*, and multiple scattering peak positions. Fig. 3a shows the Ni K-edge XANES of NiFe-LDH- Ti_4O_7, together with NiFe-LDH, NiO, and $Ni(OH)_2$ as the references. The oxidation state of as-prepared NiFe-LDH is close to +2 since the main absorption edge position coincides with that of NiO. However, the main edge position of NiFe-LDH-Ti_4O_7 shows shifts to a higher energy than NiFe-LDH, suggesting the increased oxidation state of Ni in NiFe-LDH-Ti_4O_7 due to the electron transfer from the Ni site to the Ti_4O_7 support, agreeing with the finding from XPS. The lower white line peak implies the lower unfilled state of Ni in NiFe-LDH-Ti_4O_7 compared to Ni in NiFe-LDH. Fig. 3b shows the Fe−K edge XANES spectra for NiFe-LDH and NiFe-LDH-Ti_4O_7,

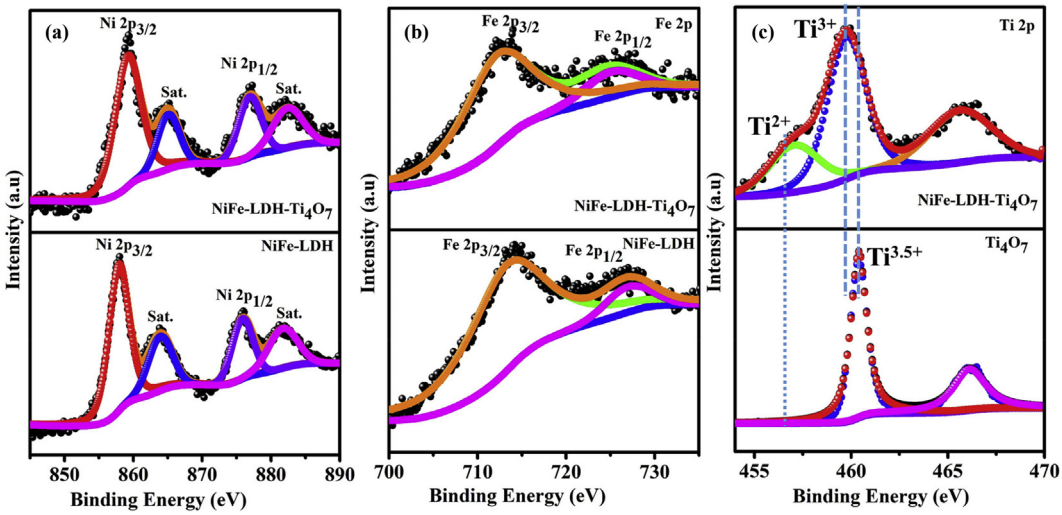

Fig. 2. XPS spectra of (a) Ni 2p, (b) Fe 2p, and (c) Ti 2p in NiFe-LDH and NiFe-LDH-Ti_4O_7.

together with reference compounds α-Fe_2O_3 and γ-Fe_2O_3. The edge position of the NiFe-LDH-Ti_4O_7 sample is slightly shifted toward higher binding energy than NiFe-LDH and the other iron oxide samples, suggesting that the oxidation of Fe in NiFe-LDH-Ti_4O_7 is higher than Fe^{3+}. It is to note that the trend of Fe oxidation state in various samples observed by XANES is different from the aforementioned XPS results. The inconsistency might result from the difference in the probing depths in the two analysis techniques.

On the other hand, the Ti K-edge in Ti_4O_7 shows shifts to lower energy relative to TiO_2, both commercial and synthesized, insinuating the partial reduction of Ti^{4+} to Ti^{3+} in Ti_4O_7. In contrast, the edge position of Ti K-edge in NiFe-LDH-Ti_4O_7 has a noticeable shift to lower energy compared to Ti_4O_7 (Fig. 3c), suggesting the valence state of Ti in NiFe-LDH-Ti_4O_7 becomes lower after the decoration. This was rationalized by the charge compensation mechanism because there is more loss of metal sites in LDH during the decorating by Ti_4O_7. In the XANES analysis, the positive and negative shifts of the (Ni, Fe) and Ti K-edge reveal the strong electronic interaction between NiFe-LDH and Ti_4O_7 when forming a heterostructured composite, whereby the electrons are primarily transferred from the Ni sites in NiFe-LDH (i.e., oxidation state from +2 to > +2) to Ti_4O_7. The coupling effect between NiFe-LDH and Ti_4O_7 regulates the redox behaviors of Ni and Fe cations, resulting in active phases during the OER process. The combination of LDH and

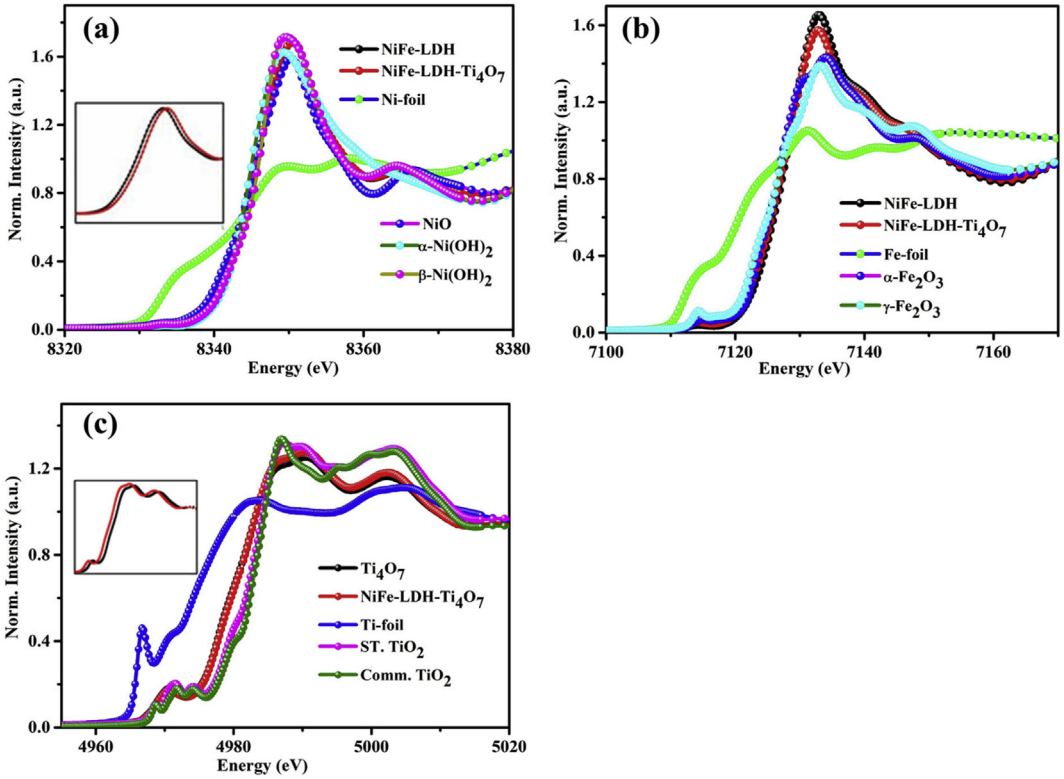

Fig. 3. XANES at the (a) Ni K-edge, (b) Fe K-edge, and (c) Ti K-edge curves of catalysts and standards.

oxide and the composite formation gives rise to some changes in the coordination environment and structural order/disorder. This evidence is believed to be associated with enhancing intrinsic properties of NiFe-LDH, which remarkably improves the OER activity of NiFe-LDH- Ti_4O_7, which will be discussed in the next section.

Tailoring the electronic structures of electrocatalysts through defect engineering (such as oxygen vacancies (Ovac) and Ni^{3+} defects) is the fundamental strategy to increase the number of active sites, shorten the electron/ion path to facilitate their transfer rates and improve the intrinsic activity, thus substantially increase OER performance [27]. Next, EXAFS spectra provide direct evidence for the as-synthesized catalyst's local structure and atomic arrangement. Thus, EXAFS spectra of Ni and Fe K-edges of both NiFe-LDH and NiFe-LDH-Ti_4O_7 display two main peaks assigned to the nearest neighbor metal−oxygen (M−O) and metal-metal (M−M) correlation, as seen in Fig. 4a and b and Fig. S6. The Ni−O EXAFS spectra for NiFe-LDH-Ti_4O_7 has a slightly lower bond length (Ni−O 1.98 Å) and coordination number (N = 5.77) (Fig. 4a, Table S1) relative to $Ni(OH)_2$ (2.06 Å, N = 6.0) and NiFe-LDH (2.03 Å, N = 5.86). Therefore, the M − O and M−M bond for Ni K-edge spectra before and after decorating by Ti_4O_7 show a negligible change in intensity (Fig. 4a), suggesting both Ni's local structure and crystalline size NiFe-LDH is not affected by decorating Ti_4O_7. Likewise, the EXAFS Fe K-edge (Fig. 4b and Table S2) in NiFe-LDH-Ti_4O_7 shows a lowered intensity of these two peaks compared to NiFe-LDH. This indicates that the NiFe-LDH-Ti_4O_7 composite contains fewer Fe cations caused by the increased number of edge defects and vacancies, as estimated by the fitting parameters summarized in Table S1. The lowered intensity of the peaks suggested that the material contained massive oxygen and metal vacancy defects, indicating structural distortion and the existence of vacancy resulting from blending Ti_4O_7. The obtained defective structure with a low coordination environment would improve the electronic conductivity and facilitate the adsorption process of H_2O onto metal cations, thereby increasing the intrinsic catalytic activity of NiOOH [28]. Further, defect-induced structural distortions can also be observed. The K-edge k^3x oscillation curve of Ni in NiFe-LDH-Ti_4O_7 (Fig. S5) demonstrated a minor change. Still, Fe's K-edge k^3x oscillation curve shows a significant change in Fe the oscillation amplitude, suggesting a change for Fe atoms' coordination environment. Concurrently, in Fig. 4c, the Ti K-edge spectra show an insignificant change in intensity before and after combining with LDH, implying that the Ti K-edge was not much affected by the combination between catalyst and support. Fig. 4d showed the schematic process with oxygen and metal multivacancies, which could be expected substantially to alter the electronic structure and enhance the electrocatalytic performance for NiFe-LDH-Ti_4O_7.

3.3. Oxygen evolution reaction

The OER is a surface practice and is considerably inclined by the surface nature of the electrocatalyst. Thus, the degree of disorder, coordination number of the surface atoms, and bond configurations in the electrocatalyst affect its electrocatalytic activity. Therefore, linear sweep voltammetry (LSV) was performed to confirm the OER electrochemical activity of NiFe-LDH-Ti_4O_7. In Fig. 5a, the polarization curve of the as-synthesized material, with an oxidation peak and onset potential for OER at ~1.38 V, and 1.43 V (vs. RHE), respectively. The best OER activity (lower onset overpotential) is ascribed to the oxidation of $Ni(OH)_2$ to NiOOH species. Interestingly, the oxidation of Ni^{2+} to Ni^{3+} NiFe-LDH-Ti_4O_7 appears at a lower overpotential than NiFe-LDH and $Ni(OH)_2$. A lower potential is required for the formation of NiOOH phase on the NiFe-LDH-Ti_4O_7 than on the NiFe-LDH and $Ni(OH)_2$, indicating the faster kinetics of the NiFe-LDH-Ti_4O_7 to realize the Ni^{2+}-Ni^{3+} transformation, corresponding to a smaller overpotential [29–31]. The much easier formation of NiOOH species in NiFe-LDH-Ti_4O_7 than that of NiFe-LDH is mainly ascribed to factors, including 1) better conductivity of Ti_4O_7, whose conductivity is much higher than

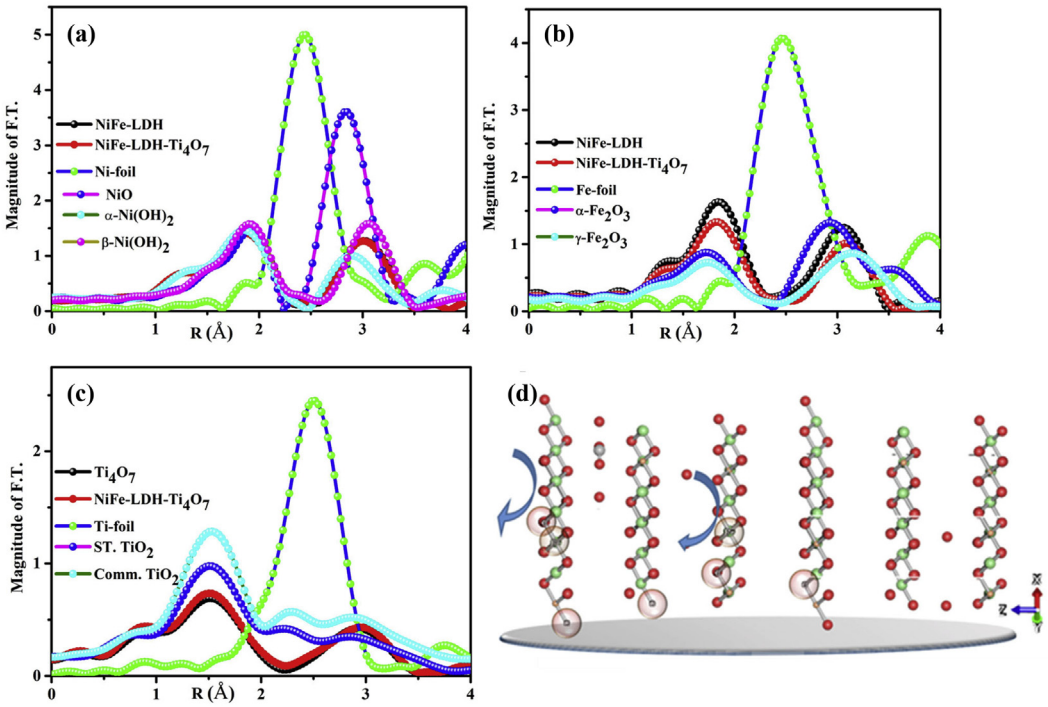

Fig. 4. EXAFS of the (a) Ni K-edge, (b) Fe K-edge, and (c) Ti K-edge curves of catalysts and standards (d) Vacancy defected NiFe-LDH-Ti_4O_7 where clear balls indicate oxygen vacancies (red hue) and Fe vacancies (orange hue). Hydroxyl ions, water molecules, and intercalated ions in the interlayers were simplified for better clarity.

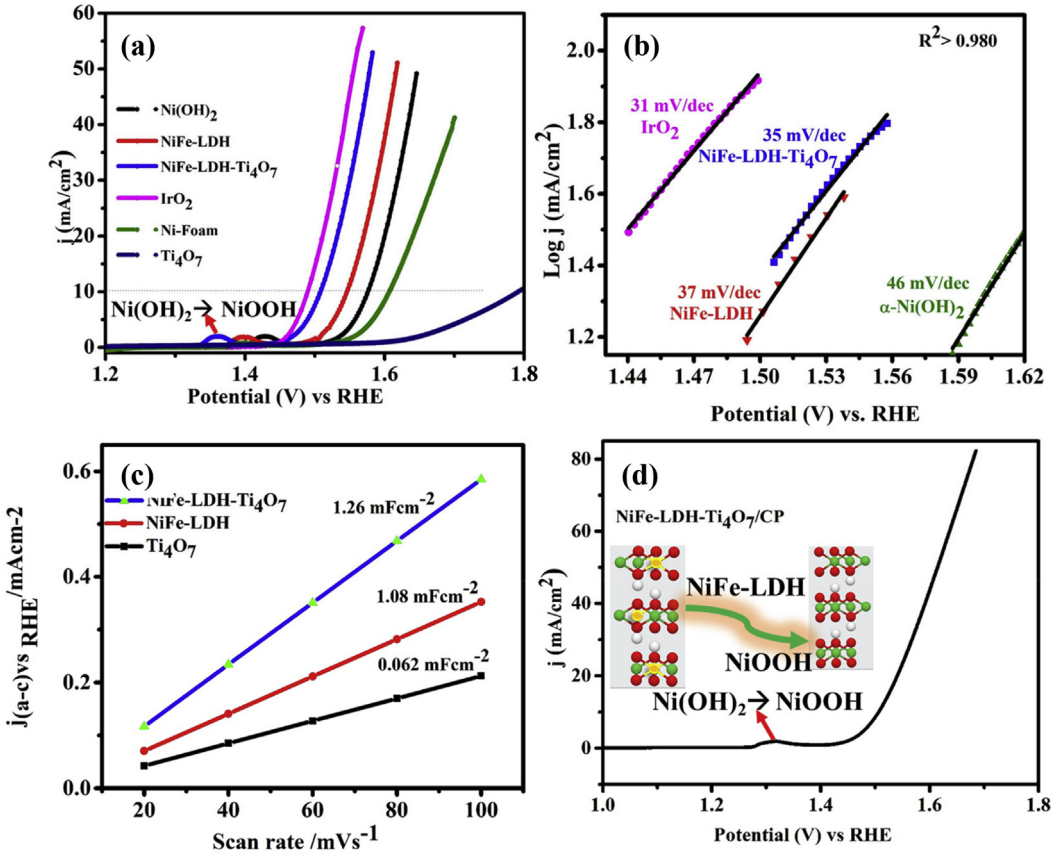

Fig. 5. (a) LSV plot of NiFe-LDH, NiFe-LDH-Ti_4O_7, Ti_4O_7, α-Ni $(OH)_2$, and $IrO_2$for OER. Scan rate: 1 mV/s; (b) The equivalent Tafel plots; (c) Current density difference plotted against scan rates; (d) LSV plot of NiFe-LDH-Ti_4O_7 drop cast on carbon paper.

anatase TiO_2 (and NiFe-LDH), which facilitates the charge transfer; 2) abundant unsaturated sites created due to the formation of a heterostructured composite, as evidenced in XAS/EXAFS analysis. Notice that Ni^{3+} reacts with water to generate oxygen. As a result, the coexistence of Ni^{3+}/Ni^{2+} species is crucial to activating water, and the OER is likely to occur at the domain Ni^{3+} sites. As confirmed in our FTIR spectra Fig. S3d, the presence of NO_3^- at around 1385 cm^{-1} resulted from metal precursors and OH^- in the electrolyte would intercalate into the interlayer galleries of LDH to maintain the charge neutrality when Ni^{2+} is transformed into Ni^{3+}. Thus, the faster and easier formation of more NiOOH involved in the reaction demonstrates faster kinetics and higher intrinsic OER activity of the NiFe-LDH-Ti_4O_7. During this measurement, there was no redox transition in Fe observed at a similar potential range. Hence, Fe in NiFe-LDH can benefit the O* radical formation, and Ni facilitates the O—O coupling, but the weak adsorption of oxygenated intermediates (especially *OH) to the NiFe-LDH is potentially the highest energy-consuming step.

To reach a current density of 10 mA/cm^2, NiFe-LDH-Ti_4O_7 required an applied overpotential of 270 mV, whereas the commercial benchmark IrO_2 could be operated at an overpotential of 260 mV. The comparable overpotential indicates that NiFe-LDH-Ti_4O_7 is efficient toward OER and can be an effective alternative to expensive IrO_2, which surpasses barely with 10 mV less. For comparison, the other two electrocatalysts, $Ni(OH)_2$ and NiFe-LDH, had overpotentials of 350 and 320 mV under the same conditions. The NiFe-LDH-Ti_4O_7 composite exhibits a lower OER overpotential than NiFe-LDH, which confirms that the heterostructured composite material is highly active for OER, most probably due to the synergistic effects between NiFe-LDH and conductive Ti_4O_7 and the increased number of active sites. To further investigate the OER reaction kinetics, the Tafel slope of each sample was estimated in Fig. 5b. A smaller Tafel slope implies a higher OER kinetics activity. It is interesting to know that the estimated Tafel slope of IrO_2, NiFe-LDH-Ti_4O_7, NiFe-LDH, and α-$Ni(OH)_2$ are 31, 35, 37, and 44 mV/dec, respectively. The estimation results show the inclusion of conductive Ti_4O_7 is beneficial for NiFe-LDH with faster charge transfer, which enhances the OER activity in return. Moreover, the catalysts' double-layer capacitance (C_{dl}) was estimated to compare the electrochemically active surface area (ECSA) of LDH samples and Ti_4O_7 by measuring the charging current in a potential window free of the Faradic process, as seen in Fig. S7. The ECSA value is presented by the linear slope of the capacitive current versus scan rate, equivalent to twice the double-layer capacity C_{dl} [29,30]. The C_{dl} values (Fig. 5c) of the catalysts were 1.08, 0.062, and 1.26 mF cm^{-2} for NiFe-LDH, Ti_4O_7, and NiFe-LDH-Ti_4O_7, respectively. It is to note that the ECSA of the heterostructured composite increased approximately 16.7% from the pristine NiFe-LDH. The large ECSA value for the NiFe-LDH-Ti_4O_7 composite is another main contributing factor to an increase in OER catalytic activity. To avoid the confusion of the contribution of Ni foam when used as a current collector, we drop cast our catalyst on carbon paper, which has no OER performance with good electronic conductivity and can release the oxygen bubbles quickly from the surface. However, the performance does not vary with NiFe-LDH-Ti_4O_7/Ni foam. Both have the same onset potential of 1.43 V, as depicted in Fig. 5d. Further, to compare synthesized catalysts' intrinsic activities, ECSA normalized LSV (Fig. S8) is provided. As a result, the intrinsic activity for NiFe-LDH-Ti_4O_7 shows an increase after taking ECSA normalization compared to NiFe-LDH [34]. Although the increased

electrochemical current in NiFe-LDH might actually be from the increased surface area, Ti_4O_7 can affect the surface area for NiFe-LDH-Ti_4O_7. As discussed in the EXAFS analysis, the decoration of Ti_4O_7 resulted in the additional generation of metal vacancies (mainly Fe sites) and oxygen vacancies, which help create and expose more active sites. As mentioned, the presence of conductive Ti_4O_7 in the LDH composite also enables a stronger electronic coupling with the electrocatalyst itself and allows faster charge transfer. More assessable active sites with improved reaction kinetics give consequently superior activity.

The electrocatalytic kinetics and charge transfer process were also investigated further through electrochemical impedance spectroscopy (EIS) of as-synthesized samples at an overpotential of 220 mV. In Fig. 6a and Table 1, NiFe-LDH-Ti_4O_7 possesses the smallest semicircle, which indicates that the composite material has the lowest R_{ct} among all samples at the corresponding electrode/electrolyte interface, pointing to a fast reaction rate of NiFe-LDH-Ti_4O_7. The R_{ct} value of NiFe-LDH is twice as high as that of the R_{ct} of NiFe-LDH-Ti_4O_7. The decorated Ti_4O_7 dramatically improves the conductivity of the NiFe-LDH and hence enhances its OER performance. Besides the activity, the durability of the electrocatalysts is another critical parameter. Then, we measured using the chronopotentiometry method at a potential of 1.45 V vs. RHE in 1 M KOH solution after drop-casting on carbon paper to avoid extra bubbles from Ni foam. During durability measurement, the increase in current density observed for the first 10 h in NiFe-LDH-Ti_4O_7 (Fig. 6b), which might be attributed to insufficient wetting of carbon paper, or an electro-activation process (i.e., phase transformation) [35], the loss of intercalated anions ions [36], and activation process of $Ni(OH)_2$ material to produce high oxidation intermediates [37,38]. The heterostructured NiFe-LDH-Ti_4O_7 composite showed satisfying durability for 30 h without noticeable degradation in the activity or structure.

Table 1
Fitting data for corresponding equivalent circuit Nyquist plots of the electrochemical impedance spectra.

Electrode	R_s (ohm)	R_{ct} (ohm)	CPE1 ($\Omega S^{-1/2}$)
NiFe-LDH	47.35	422.7	0.62
Ti_4O_7	45.77	375.2	0.76
NiFe-LDH-Ti_4O_7	46.75	106.3	0.77

To sum up the overall effects of the decoration of Ti_4O_7 and the heterostructured composite, the insertion of Fe into hexagonal nickel hydroxide, and the decoration of NiFe-LDH with Ti_4O_7 result in metal vacancies (primarily Fe) and oxygen vacancies and increased activity. Furthermore, it is known the redox transformation of Ni^{2+} to Ni^{3+} in $Ni(OH)_2$ can be seen as the activation of active sites. Hence, the required onset overpotential ratio for $Ni(OH)_2$, NiFe-LDH, and NiFe-LDH-Ti_4O_7 can be termed as a benchmarking percentage for the site activity among these electrocatalysts with a similar layered structure. As seen in Fig. 6c, the corresponding onset overpotentials for NiFe-LDH and NiFe-LDH-Ti_4O_7 require 95% and 92% of the reference sample $Ni(OH)_2$. As confirmed by XPS and XANES results, the electronic coupling in the composite is reflected by the redox transformation of Ni^{2+} to Ni^{3+}. The electron transfer from Ni to Ti_4O_7 is believed to facilitate the mechanism. Thus, a lower overpotential percentage than the reference indicates the higher site activity of the decorated material. We also propose that larger lattices (from XRD) favor the ionic intercalation of NO_3^-, OH^- and the exposure of more active sites for oxygen-evolving (Fig. 6d), which is confirmed by the increase of ECSA from $Ni(OH)_2$ → NiFe-LDH → NiFe-LDH-Ti_4O_7 (Fig. 5c). Furthermore, for NiFe-LDH-Ti_4O_7, the Ni–M (M = Ni, Fe, Ti) electronic interaction evidenced from XAS and XPS (Figs. 2 and 3) is an important factor in enhancing the catalytic activity of NiFe-LDH-Ti_4O_7.

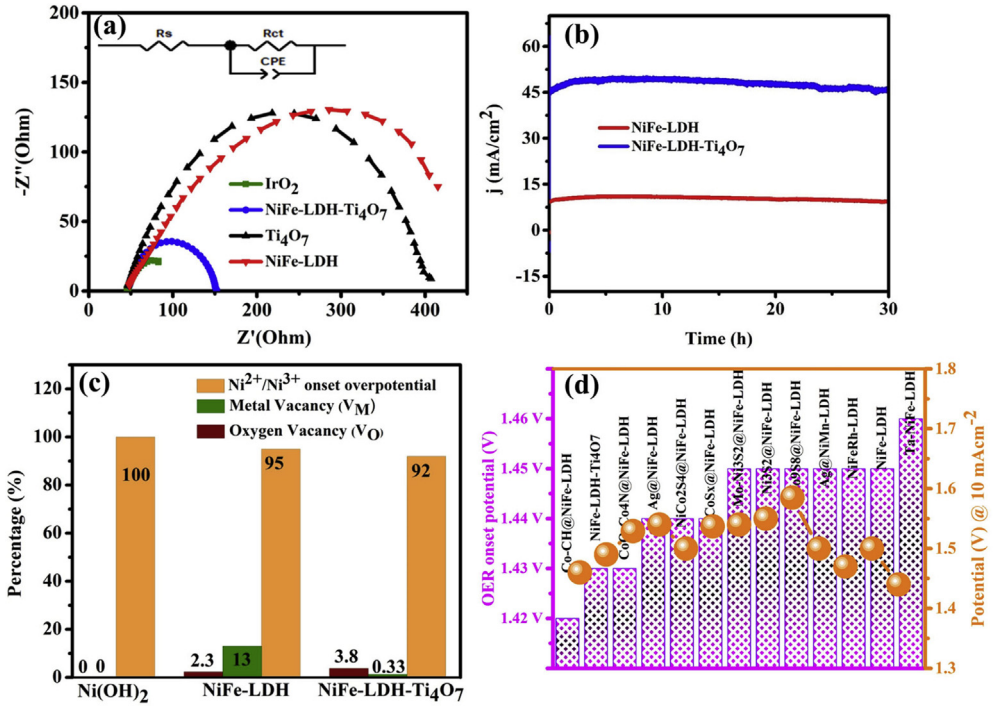

Fig. 6. (a) Nyquist spectra at an overpotential of 220 mV. Inset: the corresponding equivalent circuit; (b) Chronopotentiometry OER stability test for NiFe-LDH, NiFe-LDH-Ti_4O_7 at a potential of 1.45 V vs. RHE in 1 M KOH solution; (c) Percentage of vacancies (both oxygen and metal) and oxidation overpotential where $Ni(OH)_2$ was referred as a benchmarking sample; (d) Comparison of the OER onset potential and the cell voltages of electrocatalysts to produce 10 mA/cm^2.

Providing $Ni(OH)_2$ as the standard sample with a coordination number of 6 for both Ni and O atoms, the comparative meal vacancies (V_M) and oxygen vacancies (V_O) in LDH samples can be estimated from the EXAFS-derived parameters summarized in Table S3 and definition stated in the supporting information. The percentages of V_O for NiFe-LDH and NiFe-LDH-Ti_4O_7 are 2.3% and 3.8%. The induced V_O can decline the reference of H_2O adsorption on the surface of the catalyst, leading to increased site activity and improved OER activity of NiFe-LDH. The effect of oxygen vacancies and site activity are correlated. Although the Ti_4O_7 decoration slightly decreases V_M of NiFe-LDH-Ti_4O_7, the formation of metal vacancies also allied with the size reduction of LDHs increase the accessible active sites [32]. Therefore, the Ti_4O_7 decoration in conjunction with the Fe introduction into LDHs increases both accessible active sites and oxygen vacancies.

It is evident that both Ni and Fe (Ni—O—Fe) interactions play a critical role in optimizing the OER performance. For that reason, Ni sites with oxygen vacancies in concert with metal vacancies, created by the insertion of Fe to $Ni(OH)_2$ and strain effect from Ti_4O_7, act as the centers of water activation, favoring the dissociation of H_2O molecules through increasing active site activity in the electrocatalyst. Several NiFe-based OER electrocatalysts reported in literature (for example: Co—CH@NiFe-LDH [40], CoO—Co_4N@NiFe-LDH [41], Ag@NiFe-LDH [24], $NiCo_2S_4$@NiFe-LDH [33], CoSx@NiFe-LDH [42], Mo—Ni_3S_2@NiFe-LDH [30], Ni_3Se_2@NiFe-LDH [43], Co_9S_8@NiFe-LDH [44], Ag@NiMn-LDH [14], NiFeRh-LDH [31], NiFe-LDH [29,39], and Ta—NiFe-LDH [45]) are compared in Fig. 6d. The heterostructured composite NiFe-LDH-Ti_4O_7 has a satisfying OER activity with comparably low overpotential and retains 100% of the activity for 30 h, indicating its superior durability attributed to the Magnéli phase Ti_4O_7.

4. Conclusion

The heterostructured composite of NiFe-LDH-Ti_4O_7 has a comparably high activity toward the oxygen evolution reaction (OER) with an overpotential of 270 mV to achieve 10 mA/cm^2. Its Tafel slope is 35 mV/dec, showing superior reaction kinetics. The composite has demonstrated several advantages over the 2D NiFe-LDH. First, Ti_4O_7 anchored on NiFe-LDH provides a fast electron transport pathway, dramatically enhances the conductivity, and reduces the charge transfer resistance of the NiFe-LDH. The inclusion of Ti_4O_7 also brings more structural defects to the NiFe-LDH, as confirmed by EXAFS analysis. The increased oxygen vacancy ratio correlates well with then enhanced activity, whereby it is understood that more active sites are created and become accessible. The presence of metal and oxygen vacancies also affects the interfacial electron redistribution of the NiFe-LDH-Ti_4O_7 on the interface, which influences the adsorption of the active species and improves the catalytic activity. The XPS and XAS results confirm various valence states of Ni, Fe, and Ti. The electronic coupling with electron transfer from Ni sites in NiFe-LDH to T_4O_7 indicates that the earlier redox transformation of Ni^{2+} to Ni^{3+} effectively decreases the onset overpotential for OER. In the chronopotentiometry test at 1.45 V vs. RHE, the heterostructured composite NiFe-LDH-Ti_4O_7 can maintain its durability for 30 h. Consequently, this work gives mechanistic insights into designing non-precious, durable, and competitive OER electrocatalysts reinforced by highly conductive and robust materials.

Author contribution statement

Kassa Belay Ibrahim: conceptualization, methodology, validation, analysis, writing manuscript, **Wei-Nien Su**: data curation, visualization, analysis, editing manuscript, supervision, investigation, funding, **Meng-Che Tsai:** methodology, validation, analysis, **Amaha Woldu Kahsay:** methodology, **Soressa Abera Chala:** validation, analysis, **Mulatu Kassie Birhanu:** validation, **Jyh-Fu Lee**: analysis, **Bing Joe Hwang:** resources, data curation, supervision, project administration, editing manuscript. All authors discussed the results and commented on the manuscript.

Data availability

The raw/processed data required to reproduce these findings can be shared upon kind request by contacting the corresponding authors.

Declaration of competing interest

The authors declare that they have no known competing financial interests or personal relationships that could have appeared to influence the work reported in this paper.

Acknowledgment

Financial support from the Ministry of Science and Technology of Taiwan (MOST 110-2639-E-011-001-ASP, 110-3116-F-011-003, 110-3116-F-011-004, 109-2923-E-011-008, 109-2124-M-002-008, 109-2923-E-011-009), the Ministry of Education of Taiwan (MOE, U2RSC program 1080059), Academia Sinica (AS-KPQ-106- DDPP), as well as the supporting facilities from National Taiwan University of Science and Technology (NTUST), Instrumentation Center at National Taiwan Normal University (NTNU, MOST 110-2731-M-NMR000400), and National Synchrotron Radiation Research Center (NSRRC) are all gratefully acknowledged. Finally, we are also thankful to National Taiwan University (ESCA Lab) for XPS measurements.

Appendix A. Supplementary data

Supplementary data to this article can be found online at https://doi.org/10.1016/j.mtchem.2022.100824.

References

[1] M.K. Hubbert, Energy from fossil fuels, Science 109 (1949) 103—109.
[2] D. Larcher, J.M. Tarascon, Towards greener and more sustainable batteries for electrical energy storage, Nat. Chem. 7 (2014) 19.
[3] P. Rogers, Energy use in the developing world-a crisis of rising expectations, Environ. Sci. Technol. 25 (1991) 580—583.
[4] J.A. Turner, Sustainable hydrogen production, Science 305 (2004) 972—974.
[5] T. Hisatomi, J. Kubota, K. Domen, Recent advances in semiconductors for photocatalytic and photoelectrochemical water splitting, Chem. Soc. Rev. 43 (2014) 7520—7535.
[6] M. Ball, M. Wietschel, The future of hydrogen — opportunities and challenges, Int. J. Hydrogen Energy 34 (2009) 615—627.
[7] D. Voiry, H.S. Shin, K.P. Loh, M. Chhowalla, Low-dimensional catalysts for hydrogen evolution and Co2 reduction, Nature Reviews Chemistry 2 (2018), 0105.
[8] G.W. Crabtree, M.S. Dresselhaus, M.V. Buchanan, The hydrogen economy, Phys. Today 57 (2004) 39—44.
[9] M.S. Dresselhaus, I.L. Thomas, Alternative energy technologies, Nature 414 (2001) 332.
[10] K.B. Ibrahim, W.-N. Su, M.-C. Tsai, S.A. Chala, A.W. Kahsay, M.-H. Yeh, H.-M. Chen, A.D. Duma, H. Dai, B.-J. Hwang, Robust and conductive Magnéli phase Ti4o7 decorated on 3d-nanoflower niru-Ldh as high-performance oxygen reduction electrocatalyst, Nano Energy 47 (2018) 309—315.
[11] T.A. Shifa, K. Yusupov, G. Solomon, A. Gradone, R. Mazzaro, E. Cattaruzza, A. Vomiero, In situ-generated oxide in Sn-doped nickel phosphide enables ultrafast oxygen evolution, ACS Catal. 11 (2021) 4520—4529.
[12] Y. Ma, D. Liu, H. Wu, M. Li, S. Ding, A.S. Hall, C. Xiao, Promoting bifunctional water splitting by modification of the electronic structure at the interface of nife layered double hydroxide and Ag, ACS Appl. Mater. Interfaces 13 (2021) 26055—26063.
[13] S. Dresp, F. Dionigi, M. Klingenhof, T. Merzdorf, H. Schmies, J. Drnec, A. Poulain, P. Strasser, Molecular understanding of the impact of saline

contaminants and alkaline ph on nife layered double hydroxide oxygen evolution catalysts, ACS Catal. 11 (2021) 6800–6809.
[14] S.A. Chala, M.-C. Tsai, W.-N. Su, K.B. Ibrahim, B. Thirumalraj, T.-S. Chan, J.-F. Lee, H. Dai, B.-J. Hwang, Hierarchical 3d architectured Ag nanowires shelled with nimn-layered double hydroxide as an efficient bifunctional oxygen electrocatalyst, ACS Nano 14 (2020) 1770–1782.
[15] S.A. Chala, M.-C. Tsai, B.W. Olbasa, K. Lakshmanan, W.-H. Huang, W.-N. Su, Y.-F. Liao, J.-F. Lee, H. Dai, B.J. Hwang, Tuning dynamically formed active phases and catalytic mechanisms of in situ electrochemically activated layered double hydroxide for oxygen evolution reaction, ACS Nano 15 (9) (2021) 14996–15006.
[16] A. Sumboja, J. Chen, Y. Zong, P.S. Lee, Z. Liu, Nimn layered double hydroxides as efficient electrocatalysts for the oxygen evolution reaction and their application in rechargeable Zn-air batteries, Nanoscale 9 (2017) 774–780.
[17] K.B. Ibrahim, M.C. Tsai, S.A. Chala, M.K. Berihun, A.W. Kahsay, T.A. Berhe, W.N. Su, B.J. Hwang, A review of transition metal-based bifunctional oxygen electrocatalysts, J. Chin. Chem. Soc. 66 (2019) 829–865.
[18] M.-Q. Zhao, Q. Zhang, J.-Q. Huang, F. Wei, Hierarchical nanocomposites derived from nanocarbons and layered double hydroxides - properties, synthesis, and applications, Adv. Funct. Mater. 22 (2012) 675–694.
[19] C.V. Subban, Q. Zhou, A. Hu, T.E. Moylan, F.T. Wagner, F.J. DiSalvo, Sol–Gel synthesis, electrochemical characterization, and stability testing of Ti0.7w0.3o2 nanoparticles for catalyst support applications in proton-exchange membrane fuel cells, J. Am. Chem. Soc. 132 (2010) 17531–17536.
[20] B. Fang, N.K. Chaudhari, M.-S. Kim, J.H. Kim, J.-S. Yu, Homogeneous deposition of platinum nanoparticles on carbon black for proton exchange membrane fuel cell, J. Am. Chem. Soc. 131 (2009) 15330–15338.
[21] H. Li, H. Yang, Z. Li, X. Wang, X. Liu, S. Bandaru, X. Zhang, Vertically feni layered double hydroxide/Tio2 composite for synergistically enhanced photoelectrochemical water splitting, Electrochim. Acta 387 (2021) 138533.
[22] Y. Cao, T. Wang, X. Li, L. Zhang, Y. Luo, F. Zhang, A.M. Asiri, J. Hu, Q. Liu, X. Sun, A hierarchical Cuo@Nico layered double hydroxide core–shell nanoarray as an efficient electrocatalyst for the oxygen evolution reaction, Inorg. Chem. Front. 8 (2021) 3049–3054.
[23] Z. Wang, J. Zhang, Q. Yu, H. Yang, X. Chen, X. Yuan, K. Huang, X. Xiong, Synthesis of 3d coo nanowires supported nife layered double hydroxide using an atmospheric pressure microplasma for high-performance oxygen evolution reaction, Chem. Eng. J. 410 (2021) 128366.
[24] S.A. Chala, et al., Site activity and population engineering of niru-layered double hydroxide nanosheets decorated with silver nanoparticles for oxygen evolution and reduction reactions, ACS Catal. 9 (2019) 117–129.
[25] Y. Dou, et al., Tio2@Layered double hydroxide core–shell nanospheres with largely enhanced photocatalytic activity toward O2 generation, Adv. Funct. Mater. 25 (2015) 2243–2249.
[26] Y. Zhou, W. Zhang, J. Hu, D. Li, X. Yin, Q. Gao, Inherent oxygen vacancies boost surface reconstruction of ultrathin Ni-Fe layered-double-hydroxides toward efficient electrocatalytic oxygen evolution, ACS Sustain. Chem. Eng. 9 (2021) 7390–7399.
[27] Z. Zhao, Q. Shao, J. Xue, B. Huang, Z. Niu, H. Gu, X. Huang, J. Lang, Multiple structural defects in ultrathin nife-Ldh nanosheets synergistically and remarkably boost water oxidation reaction, Nano Res. 15 (2022) 310–316.
[28] Q. He, H. Xie, Z.u. Rehman, C. Wang, P. Wan, H. Jiang, W. Chu, L. Song, Highly defective Fe-based oxyhydroxides from electrochemical reconstruction for efficient oxygen evolution catalysis, ACS Energy Lett. 3 (2018) 861–868.
[29] D. Zhou, et al., Nife hydroxide lattice Tensile strain: enhancement of adsorption of oxygenated intermediates for efficient water oxidation catalysis, Angew. Chem. Int. Ed. 58 (2019) 736–740.
[30] X. Feng, Y. Shi, J. Shi, L. Hao, Z. Hu, Superhydrophilic 3d peony flower-like Mo-doped Ni2s3@Nife Ldh heterostructure electrocatalyst for accelerating water splitting, Int. J. Hydrogen Energy 46 (2021) 5169–5180.
[31] H. Sun, W. Zhang, J.-G. Li, Z. Li, X. Ao, K.-H. Xue, K.K. Ostrikov, J. Tang, C. Wang, Rh-engineered ultrathin nife-Ldh nanosheets enable highly-efficient overall water splitting and urea electrolysis, Appl. Catal. B Environ. 284 (2021) 119740.
[32] Q. He, Y. Wan, H. Jiang, Z. Pan, C. Wu, M. Wang, X. Wu, B. Ye, P.M. Ajayan, L. Song, Nickel vacancies boost reconstruction in nickel hydroxide electrocatalyst, ACS Energy Lett. 3 (2018) 1373–1380.
[33] X. Feng, Q. Jiao, W. Chen, Y. Dang, Z. Dai, S.L. Suib, J. Zhang, Y. Zhao, H. Li, C. Feng, Cactus-like Nico2s4@Nife Ldh hollow spheres as an effective oxygen bifunctional electrocatalyst in alkaline solution, Appl. Catal. B Environ. 286 (2021) 119869.
[34] H. Ren, Y. Pan, C.C. Sorrell, H. Du, Assessment of electrocatalytic activity through the lens of three surface area normalization techniques, J. Mater. Chem. 8 (2020) 3154–3159.
[35] A.T.A. Ahmed, S.M. Pawar, A.I. Inamdar, H. Im, H. Kim, Fabrication of Feo@Cuco2s4 multifunctional electrode for ultrahigh-capacity supercapacitors and efficient oxygen evolution reaction, Int. J. Energy Res. 44 (2020) 1798–1811.
[36] C. Feng, et al., A self-healing catalyst for electrocatalytic and photoelectrochemical oxygen evolution in highly alkaline conditions, Nat. Commun. 12 (2021) 5980.
[37] S.M. Pawar, et al., Self-assembled two-dimensional copper oxide nanosheet bundles as an efficient oxygen evolution reaction (oer) electrocatalyst for water splitting applications, J. Mater. Chem. 5 (2017) 12747–12751.
[38] S. Cui, X. Liu, Z. Sun, P. Du, Noble metal-free copper hydroxide as an active and robust electrocatalyst for water oxidation at weakly basic ph, ACS Sustain. Chem. Eng. 4 (2016) 2593–2600.
[39] Z. Lu, W. Xu, W. Zhu, Q. Yang, X. Lei, J. Liu, Y. Li, X. Sun, X. Duan, Three-dimensional nife layered double hydroxide film for high-efficiency oxygen evolution reaction, Chem. Commun. 50 (2014) 6479–6482.
[40] S. Cao, H. Huang, K. Shi, L. Wei, N. You, X. Fan, Z. Yang, W. Zhang, Engineering superhydrophilic/superaerophobic hierarchical structures of Co-Ch@Nife-Ldh/Nf to boost the oxygen evolution reaction, Chem. Eng. J. 422 (2021) 130123.
[41] B. Chen, M. Humayun, Y. Li, H. Zhang, H. Sun, Y. Wu, C. Wang, Constructing hierarchical fluffy coo–Co4n@Nife-Ldh nanorod arrays for highly effective overall water splitting and urea electrolysis, ACS Sustain. Chem. Eng. 9 (2021) 14180–14192.
[42] Y. Yang, et al., Self-supported nife-Ldh@Cosx nanosheet arrays grown on nickel foam as efficient bifunctional electrocatalysts for overall water splitting, Chem. Eng. J. 419 (2021) 129512.
[43] J. Hu, S. Zhu, Y. Liang, S. Wu, Z. Li, S. Luo, Z. Cui, Self-supported Ni3se2@Nife layered double hydroxide bifunctional electrocatalyst for overall water splitting, J. Colloid Interface Sci. 587 (2021) 79–89.
[44] Y. Lu, C. Liu, Y. Xing, Q. Xu, A.M.S. Hossain, D. Jiang, D. Li, J. Zhu, Synergistically integrated Co9s8@Nife-layered double hydroxide core-branch hierarchical architectures as efficient bifunctional electrocatalyst for water splitting, J. Colloid Interface Sci. 604 (2021) 680–690.
[45] X. Wang, Y. Tuo, Y. Zhou, D. Wang, S. Wang, J. Zhang, Ta-doping Triggered electronic structural engineering and strain effect in nife Ldh for enhanced water oxidation, Chem. Eng. J. 403 (2021) 126297.